Phase Diagram of Colloidal Solutions

Neer Asherie, Aleksey Lomakin, and George B. Benedek
Department of Physics and Center for Materials Science and Engineering, Massachusetts Institute of Technology, Cambridge, Massachusetts 02139-4307
(Received 1 July 1996)

The phase diagram of globular colloids is studied using a combined analytic and computational representation of the relevant chemical potentials. It is shown how the relative positions of the phase boundaries are related to the range of interaction and the number of contacts made per particle in the solid phase. The theory presented successfully describes the features of the phase diagrams observed in a wide variety of colloidal systems. [S0031-9007(96)01805-4]

PACS numbers: 82.70.Dd, 64.70.Ja

The phase diagrams of colloidal solutions have been studied for over a century not only because of their great theoretical interest, but also for the many industrial applications of colloids [1]. The most commonly observed phase transition in colloidal solutions is solidification. Upon a change in temperature (or other external condition) the colloidal particles form a condensed phase which may have a regular structure (crystals) or be amorphous (aggregates). A more infrequent transition is liquid-liquid phase separation (coacervation). Here the colloidal solution forms two distinct liquid phases: one colloid-rich, the other colloid-poor [2].

These transitions have analogous counterparts in simple molecular fluids. The solidification of colloids is equivalent to the fluid-solid transition while colloidal liquid-liquid phase separation corresponds to gas-liquid coexistence. There is, however, one striking difference: when most simple fluids are cooled the order of phases observed is gas to liquid to solid. In colloidal solutions the colloidal "gas" usually transforms into a solid without passing through a liquid phase.

We illustrate this "anomalous" order of phases by presenting in Fig. 1 the phase diagram of γ_{II}-crystallin protein [3–5]. This phase diagram is typical of the γ-crystallins (a family of monomeric eye lens proteins) and of other small globular proteins [6–8]. The circles are points which represent the volume fractions (ϕ) of coexisting protein-rich and protein-poor liquid phases (liquid-liquid coexistence curve). The squares (liquidus line) and the triangle (solidus line), respectively, represent the volume fractions of protein in the liquid and solid phases in equilibrium with each other. We see that there is no triple point and the coexistence curve lies below the liquidus line. The γ-crystallins are an unusual colloidal system in that liquid-liquid phase separation may be observed despite it being metastable with respect to solidification. For comparison the phase diagram of argon is shown in Fig. 2 [9–11]. We see that for argon the critical point lies above the triple point (i.e., $T_c > T_t$) indicating the presence of a stable liquid phase. Although most colloidal phase diagrams resemble that shown in Fig. 1, a few do show phase behavior closer to that pictured in Fig. 2 [12].

Recently, evidence has accumulated that the interaction range plays a significant role in determining the structure of the phase diagram [13]. In colloid-polymer mixtures it has been found that the shape of the phase diagram depends on the ratio of the radius of gyration of the polymer molecules to the radius of the colloidal particles [12,14,15]. Theoretical models [16,17] of this system agree with the experimental observation that with very small polymers (i.e., very short ranges of attraction) there is no colloidal liquid phase [12]. Colloids are not the only system for which the connection between short-range interactions and the structure of the phase diagram has been noted. Fullerenes, macromolecules of carbon, also do not appear to exhibit a liquid phase upon cooling [18]. Simulations of hard spheres with an attractive Yukawa potential have been carried out to investigate the phase diagram of the fullerene C_{60} [19,20]. It is found that for

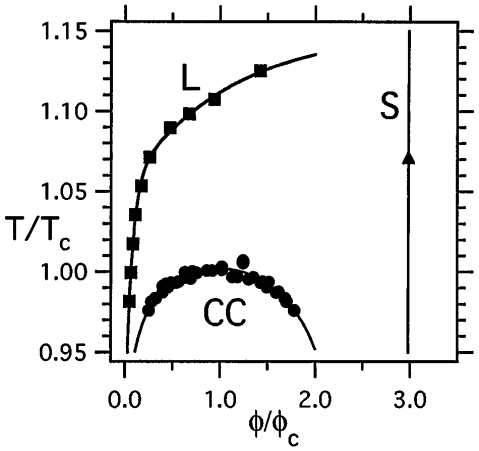

FIG. 1. The phase diagram of γ_{II}-crystallin [3–5]. The circles are points on the liquid-liquid coexistence curve (CC). The squares are points on the liquidus line (L). The triangle is a point on the solidus line (S). The lines are guides to the eye. The critical temperature is $T_c = 278.4$ K. The critical volume fraction is $\phi_c = 0.21$.

 0031-9007/96/77(23)/4832(4)$10.00

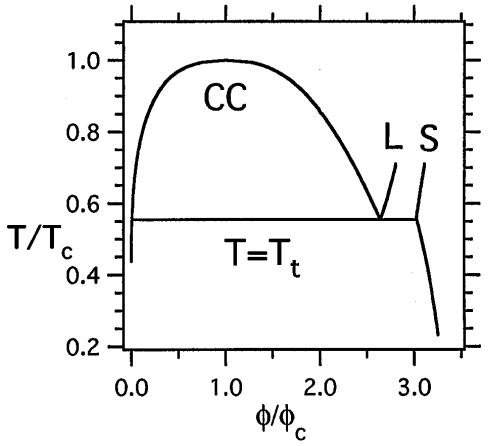

FIG. 2. The phase diagram of argon [9–11] showing the coexistence curve (CC) and the liquidus (L) and solidus (S) lines. The critical temperature is $T_c = 150.86$ K. The critical volume fraction is $\phi_c = 0.133$, assuming a hard core diameter $\sigma = 3.162$ Å [29]. The triple point temperature is $T_t = 83.78\ \mathrm{K} = 0.56 T_c$.

a sufficiently short-range potential the coexistence curve lies below the liquidus curve.

In this Letter we present a general analysis which explains these individual experimental and theoretical findings. In our previous Monte Carlo work [21] we studied the liquid-liquid phase separation of globular particles with attractive interactions and obtained numerically the chemical potential of the *liquid* phase. Here we present an analytic expression for the chemical potential of a *solid* with short-range interactions. Our model of the solid incorporates the same essential features that were used to describe the liquid phase: the range λ of the interaction, the interaction energy ϵ, and the number of contacts n_s made per particle. Knowing the chemical potentials of both phases we are able to demonstrate how the relative locations of the phase boundaries are related to λ and n_s.

We use the Lennard-Jones and Devonshire cell model [22] to obtain an approximate analytic expression for the chemical potential of a solid with short-range interactions. As in our previous work, we will assume that the effective potential energy $u(r)$ for a pair of proteins (diameter σ) whose centers are separated by a distance r, is of the form of an attractive square well with a hard core as given by

$$u(r) = \begin{cases} +\infty, & \text{for } r < \sigma\,, \\ -\epsilon, & \text{for } \sigma \le r < \lambda\sigma\,, \\ 0, & \text{for } r \ge \lambda\sigma\,. \end{cases} \qquad (1)$$

Here λ is the reduced range of the potential well and ϵ is its depth. When the interactions are short ranged ($\lambda \to 1$) the thermodynamic properties become universal, independent of the shape of the potential. We work with the square-well potential rather than other potentials [19,20,23] because it allows for an unambiguous definition of not only the range of interaction λ, but also of n_s, the number of contacts made per particle in the solid phase. Explicitly, n_s is the number of particles whose centers lie in the region $\sigma \le r < \lambda\sigma$ from a given particle. The square-well model produces a very simple form for the chemical potential of the solid μ_s, namely,

$$\mu_s = \mu_0 - n_s(\epsilon/2) - kT \ln[(\lambda - 1)^3]\,. \qquad (2)$$

The first term on the right-hand side of Eq. (2), μ_0, is the standard part of the chemical potential. The second term is the total energy associated with each particle. The last term is the entropic contribution: the volume accessible to the center of mass of the particle is proportional to $(\lambda - 1)^3$. The proportionality factor, essentially the volume of a unit cell, has been absorbed into μ_0. This factor can be calculated within the framework of the cell model [24]. The cell volume, however, is practically constant, reflecting the incompressibility of the solid phase. We may therefore choose a cell volume at zero pressure. The corresponding value of μ_0 is found to be identical to that in the expression $\mu = \mu_0 + kT \ln \phi$, which is appropriate for dilute solutions [25].

An important parameter in the chemical potential of the solid is n_s. The value of n_s is not known *a priori*, but determined by the structure of the solid. It is common practice to impose a particular crystal structure upon the solid when calculating the chemical potential by choosing the appropriate integral value for n_s. In the subsequent analysis, however, we will treat n_s as a continuous, phenomenological parameter so as to subsume within the cell model the actual structure and detailed interactions in the solid phase of real colloids.

The liquidus line is obtained by equating the chemical potentials of the solid and the liquid, namely,

$$\hat{\mu}_s(\hat{\epsilon}; n_s) = \hat{\mu}_l(\phi, \hat{\epsilon})\,. \qquad (3)$$

Here $\hat{\mu}_s \equiv [\mu_s - \mu_0]/kT$ and thus

$$\hat{\mu}_s = -n_s(\hat{\epsilon}/2) - 3\ln[(\lambda - 1)] \qquad (4)$$

is the reduced chemical potential of the solid. The reduced chemical potential of the liquid $\hat{\mu}_l$ has been previously established as a numerical function of ϕ and $\hat{\epsilon}$ [21] ($\hat{\epsilon} \equiv \epsilon/kT$ is the reduced energy).

For any solid with a given value of n_s, Eq. (3) allows us to construct the liquidus line. In Fig. 3 we show the liquidus lines for several values of n_s at $\lambda = 1.25$: $n_s = 12.0$ (A); $n_s = 11.6$ (B); $n_s = 11.5$ (C). The line (D) is the solidus line obtained by using the volume of a unit cell appropriate to a face-centered cubic solid ($n_s = 12$) at zero pressure [24]. The coexistence curve (E) is taken from our previous work [21]. As the value of n_s increases liquid-liquid coexistence becomes metastable with respect to solidification. The shape of the phase diagram for $n_s = 12.0$ (curves A, D, and E) has the same structure as the one found experimentally for the γ-crystallins (Fig. 1).

We may consider as a measure of the metastability of the liquid phase the "metastability gap" $(T_L - T_c)/T_c$,

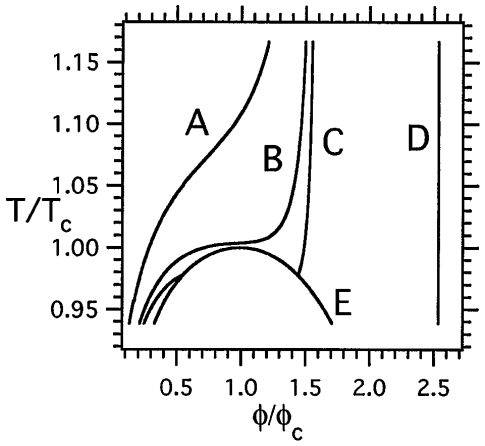

FIG. 3. The phase diagram for a square-well system for $\lambda = 1.25$. The liquidus lines for three values of n_s are shown: $n_s = 12.0$ (A); $n_s = 11.6$ (B); $n_s = 11.5$ (C). The vertical line (D) is the solidus for $n_s = 12.0$. Curve E is the coexistence curve taken from Ref. [21].

where T_c is the critical temperature and T_L is the temperature of the point on the liquidus line at the critical volume fraction ϕ_c. According to Eq. (3)

$$\hat{\mu}_s(\hat{\epsilon}_L; n_s) = \hat{\mu}_l(\phi_c, \hat{\epsilon}_L), \tag{5}$$

with $\hat{\epsilon}_L = \epsilon/kT_L$. As we have shown earlier [21], the chemical potential of the liquid at $\hat{\epsilon}_L$ may be expanded about the reduced critical energy $\hat{\epsilon}_c$

$$\hat{\mu}_l(\phi_c, \hat{\epsilon}_L) = \hat{\mu}_l(\phi_c, \hat{\epsilon}_c) - \frac{(\hat{\epsilon}_L - \hat{\epsilon}_c)}{2} n_l . \tag{6}$$

Here n_l is the change in the total number of contacts in the liquid phase upon the addition of an extra particle at the critical point. Let us define n_s^* as the number of contacts in the solid at which $T_L = T_c$, i.e., the value of n_s for which the liquidus line touches the critical point. Thus n_s^* is given by $\hat{\mu}_s(\hat{\epsilon}_c; n_s^*) = \hat{\mu}_l(\phi_c, \hat{\epsilon}_c)$. Using this definition of n_s^* and substituting Eqs. (6) and (4) into Eq. (5) we obtain

$$\frac{T_L - T_c}{T_c} = \frac{n_s - n_s^*}{n_s^* - n_l} . \tag{7}$$

From Eq. (7) we see that the metastability gap $(T_L - T_c)/T_c$ depends on the parameters n_s, n_s^*, and n_l. The first of these is determined by the structure of the solid. We list the other two in Table I. In Table I we show for each value of λ the corresponding values of n_s^* and n_l. Since n_s^* and n_l are evaluated at the critical point, these two parameters depend only on λ and not on ϵ. We note that for all of our short-range simulations, the quantity $n_s^* - n_l$ is in the range 3.2–3.8. We also list the critical volume fraction ϕ_c and the reduced critical energy $\hat{\epsilon}_c$ at each range. Columns 3–5 are from our previous work [21], while n_s^* is obtained from a numerical solution of the equation $\hat{\mu}_s(\hat{\epsilon}_c; n_s^*) = \hat{\mu}_l(\phi_c, \hat{\epsilon}_c)$.

For the solid phase to be more stable than any coexisting liquid phases i.e., $T_L > T_c$, we require $n_s > n_s^*$. The maximum number of contacts for hard spheres with short-range interactions is 12. Therefore at any given range the solid will always be stable if $12 \geq n_s > n_s^*$. As the range decreases so does n_s^* and fewer contacts are necessary to form a stable solid. Thus, we expect that as the range decreases, liquid-liquid phase separation will be less likely to be observed.

TABLE I. Metastability gap parameters at different reduced ranges λ [see Eq. (7)]. The quantities presented are (i) the average number of contacts per particle in the solid n_s^* at the metastability boundary ($T_L = T_c$), (ii) the change in the total number of contacts per particle in the liquid n_l upon the addition of an extra particle, (iii) the critical volume fraction ϕ_c, and (iv) the reduced critical energy $\hat{\epsilon}_c$.

λ	n_s^*	n_l	ϕ_c	$\hat{\epsilon}_c$
1.25	11.59	7.84	0.205	1.269
1.20	11.03	7.47	0.216	1.443
1.15	10.45	7.00	0.227	1.673
1.10	9.75	6.57	0.244	2.038
1.05	8.95	5.62	0.246	2.667

With our approach we may understand the experiments of Ilett *et al.* [12]. These authors study colloid-polymer mixtures with different ranges of interaction and find at $\lambda \approx 1.25$ a transition from the type of phase diagram shown in Fig. 2 to that in Fig. 1 (they do not observe the metastable liquid-liquid coexistence). In our analysis this transition occurs when the metastability gap changes sign, i.e., when $n_s^* = n_s$. In the solid phase the colloid-polymer system forms close-packed crystals, i.e., $n_s = 12$ [26]. Thus from Table I we expect the transition to occur at $\lambda \approx 1.25$, the value observed experimentally. In their experiments only one range of interaction shorter than the crossover value of $\lambda \approx 1.25$ is studied: $\lambda = 1.08$ [27]. Taking $n_s = 12$, Table I implies that at this range the metastability gap of the system is so large that the coexistence curve lies outside the experimentally examined region. It would be interesting to search intermediate ranges, i.e., $1.08 < \lambda < 1.25$, for metastable liquid-liquid coexistence and compare the values of the metastability gaps with our predictions.

We had previously suggested that the large values of ϕ_c and the broad coexistence curves observed for the γ-cystallins imply that these proteins lie in the domain $\lambda \leq 1.25$ [21]. We now find that this is precisely the domain where liquid-liquid coexistence may be metastable, and, in fact, this metastability is observed. When plotted in reduced units the phase diagrams of the γ-crystallins have the same shape with almost identical values of ϕ_c and with approximately the same size metastability gaps [3,21]. The interactions between these proteins may therefore be described by potentials with the same range. In addition, all the protein crystals should have the same value of n_s. For $(T_L - T_c)/T_c \approx 0.1$, the relation found experimentally for the γ-crystallins [3], Eq. (7)

gives $n_s - n_s^* \approx 0.35$. It is because n_s differs little from n_s^* that we observe both liquid-liquid coexistence and solidification for the γ-crystallins.

Related observations are made by Broide *et al.* [6] who find that the metastability gap of lysozyme is unaffected by ionic strength but that it is a larger (by 5 °C–10 °C) with respect to needle-shaped crystals than with prism-shaped crystals. In our analysis these two types of crystals are predicted to have values of $n_s - n_s^*$ differing by approximately 0.05–0.1.

It has been argued that in the adhesive sphere limit ($\lambda \to 1, \hat{\epsilon} \to \infty$) there is no thermodynamically stable liquid phase [28]. Our analysis shows that for a close-packed system the absence of a stable liquid phase already begins when $\lambda < 1.25$.

We have presented a simple analytic form for the chemical potential of a short-range solid in terms of the physically significant parameters of the system: the interaction range λ, the interaction energy ϵ, and the number of contacts made per particle n_s. We have shown how these parameters determine the order of phases found in the phase diagram. In particular, we have demonstrated that for given n_s, a sufficiently short range of interaction leads to the metastability of liquid-liquid coexistence with respect to solidification. Conversely, experimental information on the relative order of the phase boundaries of colloidal solutions gives direct insight into the magnitude of the physically important parameters λ and n_s. The theory we have presented appears capable of explaining the phase diagrams observed in a wide variety of colloidal systems.

We thank Dr. George Thurston and Dr. Jayanti Pande for critical comments. This work was supported by the National Eye Institute of the National Institute of Health under Grant No. 5-R37-EY05127.

[1] D. H. Everett, *Basic Principles of Colloid Science* (Royal Society of Chemistry, London, 1988).
[2] *Colloid Stability*, edited by D. A. Young, Faraday Discussions of the Chemical Society Vol. 65 (Chemical Society, London, 1978).
[3] C. R. Berland *et al.*, Proc. Natl. Acad. Sci. U.S.A. **89**, 1214 (1992).
[4] M. L. Broide *et al.*, Proc. Natl. Acad. Sci. U.S.A. **88**, 5660 (1991).
[5] J. A. Thomson *et al.*, Proc. Natl. Acad. Sci. U.S.A. **84**, 7079 (1987).
[6] M. L. Broide, T. Tominc, and M. Saxowsky, Phys. Rev. E **53**, 6325 (1996).
[7] D. Rosenbaum, P. C. Zamora, and C. F. Zukoski, Phys. Rev. Lett. **76**, 150 (1996).
[8] M. Muschol *et al.*, in *Photon Correlation and Scattering*, 1996 OSA Technical Digest Series Vol. 14 (Optical Society of America, Washington, DC, 1996), pp. 145–147.
[9] V. A. Rabinovich *et al.*, *Thermophysical Properties of Neon, Argon, Krypton, and Xenon* (Hemisphere, Washington, 1988), pp. 380–383.
[10] O. G. Peterson, D. N. Batchelder, and R. O. Simmons, Phys. Rev. **150**, 703 (1966).
[11] P. Flubacher, A. J. Leadbetter, and J. A. Morrison, Proc. Phys. Soc. **78**, 1449 (1961).
[12] S. M. Ilett *et al.*, Phys. Rev. E **51**, 1344 (1995).
[13] A. Daanoun, C. F. Tejero, and M. Baus, Phys. Rev. E **50**, 2913 (1994).
[14] F. Leal Calderon, J. Bibette, and J. Biais, Europhys. Lett. **23**, 653 (1993).
[15] P. N. Pusey *et al.*, J. Phys. A **6**, 29 (1994).
[16] H. N. W. Lekkerkerker *et al.*, Europhys. Lett. **20**, 559 (1992).
[17] A. P. Gast, C. K. Hall, and W. B. Russel, J. Colloid Interface Sci. **96**, 251 (1983).
[18] P. A. Heiney *et al.*, Phys. Rev. Lett. **66**, 2911 (1991).
[19] E. Lomba and N. G. Almarza, J. Chem. Phys. **100**, 8367 (1994).
[20] M. H. J. Hagen and D. Frenkel, J. Chem. Phys. **101**, 4093 (1994).
[21] A. Lomakin, N. Asherie, and G. B. Benedek, J. Chem. Phys. **104**, 1646 (1996).
[22] J. E. Lennard-Jones and A. F. Devonshire, Proc. R. Soc. London Sect. A **163**, 53 (1937).
[23] J. P. K. Doye and D. J. Wales, Science **271**, 484 (1996).
[24] J. A. Barker, *Lattice Theories of the Liquid State* (Pergamon Press, Oxford, 1963).
[25] E. A. Guggenheim, *Thermodynamics* (North-Holland, Amsterdam, 1967), 5th ed., pp. 220–224.
[26] P. N. Pusey *et al.*, Phys. Rev. Lett. **63**, 2753 (1989).
[27] W. C. K. Poon *et al.*, J. Phys. II (France) **3**, 1075 (1993).
[28] G. Stell, J. Stat. Phys. **63**, 1203 (1991).
[29] J. O. Hirschfielder, C. F. Curtiss, and R. B. Bird, *Molecular Theory of Gases and Liquids* (Wiley, New York, 2nd printing, 1964), p. 160.